J. Chem. Thermodynamics 81 (2015) 245–252

Contents lists available at ScienceDirect

J. Chem. Thermodynamics

journal homepage: www.elsevier.com/locate/jct

# High temperature phase transition of mixed ($PuO_2$ + $ThO_2$) investigated by laser melting

R. Böhler [a,b], P. Çakır [c,a], O. Beneš [a], H. Hein [a], R.J.M. Konings [a], D. Manara [a,*]

[a] European Commission, Joint Research Centre, Institute for Transuranium Elements (ITU), P.O. Box 2340, 76125 Karlsruhe, Germany
[b] Delft University of Technology, Faculty of Applied Sciences, Department of Radiation Science and Technology, Mekelweg 15, 2629 JB Delft, The Netherlands
[c] Ege University, Institute of Nuclear Sciences, 35100 Bornova Izmir, Turkey

ARTICLE INFO

*Article history:*
Received 17 July 2014
Received in revised form 29 September 2014
Accepted 5 October 2014
Available online 25 October 2014

*Keywords:*
Actinide alloys and compounds
Phase transitions
Phase diagrams
(Thorium + plutonium) dioxide

ABSTRACT

A laser heating approach combined with fast pyrometry in a thermal arrest method was used to provide new data for the melting/solidification phase transition in mixed ($PuO_2$ + $ThO_2$) at high temperature. At low concentration of $ThO_2$ in $PuO_2$ a minimum in the solidification temperature in the pseudo binary ($PuO_2$ + $ThO_2$) was observed. The minimum was found around a composition with 5 mol% $ThO_2$. Phase transition temperatures of other compositions are closer to an ideal solution behaviour. To detect changes in the material a complete investigation with electron microscopy, Raman spectroscopy and powder X-ray diffraction was done. Raman vibration modes were found, that are characteristic for materials containing $PuO_2$, and high temperature segregation effects during solidification were described. The results obtained in the present work are compared to other mixed actinide dioxides and compared to the ideal solution case for this system. The presented results show the importance of the high-temperature oxygen chemistry in this actinide oxide phase.


## 1. Introduction

Mixed actinide dioxides are a solid solution of the two dioxide end-members with a fluorite-like structure (fcc, $Fm\bar{3}m$) [1]. Thermal material properties of such systems seem to behave ideally at temperatures well below melting [1], which is shown, for example, for the $(Pu,Th)O_2$ solid solution with new heat capacity studies by Valu *et al.* [2]. Recent studies on the melting of mixed actinide dioxides ($(U,Pu)O_2$ [3], $(U,Th)O_2$ [4]) showed on the other hand a non-ideal behaviour for the high temperature melting/solidification phase transition. Both mixed systems revealed a minimum temperature in the pseudo-binary section and question the validity of an ideal solution assumption for these systems at high temperatures. These oxides, being very sensitive to the oxygen potential, then should be better regarded as ternary systems, especially at high temperatures.

The mixture of $PuO_2$ with $ThO_2$ is interesting in this context for several reasons: (i) The melting points of the pure components are the furthest apart among the actinide dioxides, that are known to be stable under standard conditions and can be used in such a melting study. (ii) The difference in ionic radius of the actinides is the largest compared to already measured binary actinide dioxide systems. (iii) The valence state is neither for Pu nor for Th in a dry environment expected to reach 5+ in contrast to uranium-containing systems. But for a given O/M ratio, the oxygen potential of $PuO_2$ is higher than other $MO_2$ phases (M = Th, U, Np). $PuO_2$ is therefore possibly easier to be reduced to a 3+ state [5]. (iv) Finally, only two basic assessments exist for the high temperature region [6,7] which also have to be updated with the newer results for $PuO_2$ [8].

In general, $(Pu,Th)O_2$ represents a potential nuclear fuel material, for which the high temperature behaviour is a fundamental parameter for the safety evaluation. Thorium dioxide based fuels could be used to reduce the long term radiotoxicity of the spent fuel by fissioning the transuranium elements [9] and is still being tested for these purposes [10]. In addition, $ThO_2$ has favourable material properties in terms of a nuclear fuel: proliferation, waste concerns and operating conditions can be improved compared to uranium based fuels [11].

It is therefore interesting to assess fundamental properties of this system and compare them to other mixed actinide dioxides. In the present work laser melting was used to study the melting/solidification behaviour. Possible effects in the material during these high temperature experiments such as segregation or stoichiometric changes have been investigated after cooling by scanning electron microscopy (SEM), Energy-dispersive X-ray

* Corresponding author.
*E-mail address:* dario.manara@ec.europa.eu (D. Manara).
*URL:* https://ec.europa.eu/jrc/en/institutes/itu (D. Manara).

http://dx.doi.org/10.1016/j.jct.2014.10.006
0021-9614/

spectroscopy (EDX), X-ray diffraction (XRD) and Raman spectroscopy. In that context, Raman spectroscopy has been used for the first time to characterise this compound. Finally, the ($PuO_2$ + $ThO_2$) pseudo-binary phase diagram was refined with new experimental high temperature phase transformation data.

## 2. Experiments

### 2.1. Sample preparation

The samples were produced using a sol-gel external gelation method with different molar fractions of $ThO_2$ ($x(ThO_2)$ = 0.05, 0.15, 0.46, 0.70, 0.92, 0.97). Samples from the same batch with 70, 92 and 97 mol% $ThO_2$ were used already for thermal diffusivity and conductivity studies [12], whereas samples with 15, 46, 70, 92 and 97 mol% $ThO_2$ were used for heat capacity studies [2]. Material with 70, 92 and 97 mol% $ThO_2$ was produced in the period of the 5th framework program of the European Commission [13,14], while samples with 5, 15 and 46 mol% $ThO_2$ were fabricated in a similar way before the melting experiments. Details about the sample preparation can be found in the aforementioned material property studies [2,12].

### 2.2. Laser melting experimental setup

The experimental apparatus used in this work was described in detail elsewhere (e.g. [4,15,16]). Only the main aspects of the setup and differences to recent work [4] are presented.

In laser melting experiments the molten volume is held by the outer periphery of the colder solid material, thus, preventing contamination by foreign material. Hence the method can be described as quasi-containerless.

The samples were preheated with low laser power (45 W) for 30 s to reduce the effect of thermal shocks. After this time a steady state heat distribution through the sample with a measured front surface temperature of (1500 to 2000) K was established and the sample was brought to melting with pulses of different length (100 ms to 1 s) at a constant power plateau (up to 1200 W). The chosen power depends also on the composition of the sample since $ThO_2$ is in the near infra-red (laser wavelength = 1064 nm) nearly transparent. This transparency is temperature-dependent and disappears at high temperature where absorption/emissivity values become similar to other actinide dioxides [17]. After each pulse the power was set back 45 W to let the sample re-solidify and reach again a surface temperature below 2000 K before the next pulse was started one second later. A maximum of 4 pulses were applied in a set of shots before letting the sample cool naturally. Such heating cycles were performed under air slightly pressurised up to 0.3 MPa to reduce vaporisation.

The surface radiance temperature in the centre of the heated zone was measured by a pyrometer operating at 652 nm with a nominal spot size of approximately 0.5 mm in diameter. The onset of melting was detected by the appearance of vibrations in the signal of a probe laser ($Ar^+$, cw, 1.5 W) reflected by the sample surface (reflected-light-signal technique, or RLS) [16]. These vibrations disappear during cooling at the thermal arrest and therefore also establish the temperature at the thermal arrest as the solidification temperature.

The true temperature was obtained by correcting the radiance temperature with the measured normal spectral emittance NSE ($\varepsilon(\lambda, T)$) with a further spectrometer, based on a linear array of 256 photodiodes (488 to 1011) nm. The measured radiance spectra can be fitted by the radiance temperature, $T_\lambda$, calculated with Wien's approximation of Planck's law and plotted as a function of wavelength, $\lambda$, assuming a grey body with constant wavelength independent emissivity $\varepsilon(T)$. For $PuO_2$ and $ThO_2$ the already published data were used (0.83 for $PuO_2$ [18]; 0.87 for $ThO_2$ [4]). Since the emittance study could not be performed on all compositions, a linear interpolation between the two NSEs of $PuO_2$ and $ThO_2$ was made, giving to the intermediate composition a weighted value related to the amount of the two end members, which are shown in table 1. This assumption seems reasonable especially considering the close emittance values of the two end members and agreed with the measured values for some intermediate compositions.

The sample surface was considered to be smooth, as supported by the good repeatability of the measured radiance temperatures upon solidification. The solidification temperature of $(Pu,Th)O_2$ was determined from the cooling stage of the recorded thermograms, locating the corresponding thermal arrest. As often observed in rapid laser-heating experiments of such materials, and confirmed by numerical simulation [19], the heating stage often occurs too quickly to reveal an observable melting arrest during this phase of the thermal cycle but could be estimated with the help of the RLS. In general, the obtained temperatures with the RLS upon heating are similar to the ones during cooling [3,4].

Uncertainties of the measurements were calculated according to the error-propagation law, taking into account the uncertainty associated to pyrometer calibration, emissivity, transmittance of the optical system and the accuracy in detecting the onset of vibrations in the reflected light signal. The estimated cumulative uncertainty is thus lower than 2% of the reported temperatures in the worst cases for the solidification temperatures (calculated a combined expanded uncertainty $U$ with a 0.95 level of confidence ($k \approx 2$)).

### 2.3. Material characterisation

To check the composition, the material was investigated with different methods before and after the experiments. First, secondary electron (SE) and backscattered electron (BSE) images were recorded on a scanning electron micro-scope (SEM with a Philips XL40®) operated at 25 kV.

Additionally, the samples were characterised with a Bruker D8 advance®X-ray diffractometer (Cu $K_\alpha$ radiation), using a range of 10° to 120° with 0.009 steps. The measurement was later also conducted on re-solidified material to see a possible effect from melting.

The third method used was Raman spectroscopy. Raman spectra were measured with a Jobin –Yvon® T64000 spectrometer used in the single spectrograph configuration. The excitation source was a Coherent®cw laser ($Ar^+$ or $Kr^+$) radiating at wavelengths of (488, 514.5, 647, and 752) nm. Spectra are measured in a confocal microscope with a 50x magnification and long focal distance (about 1 cm) with a spatial resolution of 2 · 2 μm on the sample surface.

## 3. Results

### 3.1. Melting experiments

A typical temperature versus time curve obtained with the laser melting setup is shown in figure 1. Details of the suggested interpretation can be found in earlier publications [4,3,19]. The local maximum temperature at the thermal arrest was taken as the solidification temperature of the surface. A flat thermal arrest was not observed for any of the actinide oxides, since the molten surface solidifies very quickly and builds a crust upon the molten material in only a few milliseconds. The solidification happens very quickly compared to the duration of a heating cycle. The solidification arrest can only be seen in the inset of figure 1 in which time resolution has been increased.

**TABLE 1**
Interpolated and measured normal spectral emittance (NSE),[a] and solidification temperatures[a] observed by thermal arrest analysis in this work on mixed $(Pu,Th)O_2$ at pressure $p = 0.3$ MPa.[a]

| Composition | Interpolated NSE | Measured NSE | No. of shots | Solidification temperature/K |
|---|---|---|---|---|
| $PuO_2$ | 0.830 | | | 3050 ± 55 K [3] |
| $(Pu_{0.95}Th_{0.05})O_2$ | 0.832 | 0.83 | 25 | 3008 ± 45 K |
| $(Pu_{0.85}Th_{0.15})O_2$ | 0.838 | 0.82 | 23 | 3050 ± 49 K |
| $(Pu_{0.54}Th_{0.46})O_2$ | 0.846 | 0.86 | 17 | 3208 ± 55 K |
| $(Pu_{0.30}Th_{0.70})O_2$ | 0.854 | | 2 | |
| $(Pu_{0.08}Th_{0.92})O_2$ | 0.862 | 0.90 | 6 | 3551 ± 68 K |
| $(Pu_{0.03}Th_{0.97})O_2$ | 0.868 | | 3 | 3592 ± 67 K |
| $ThO_2$ | 0.870 | | | 3624 ± 86 K [4] |

[a] Standard uncertainties $u$ are $u(p) = 0.005$ MPa, $u_r(NSE) = 0.05$, and the combined expanded uncertainty for the temperature, $U(T)$, is given for each case with a confidence level of 0.95 ($k \approx 2$).

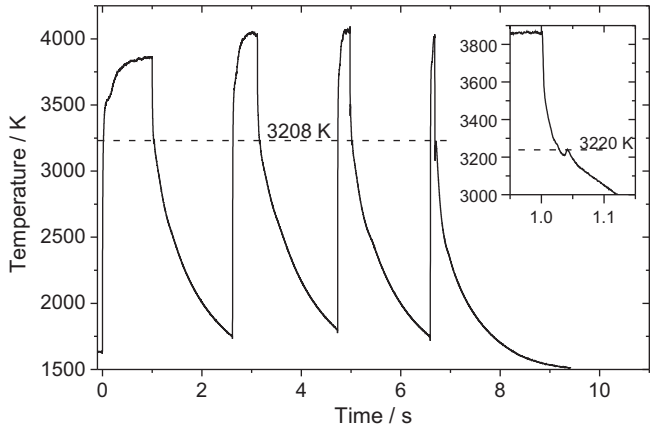


**FIGURE 1.** A sequence of four laser heating pulses performed on $(Pu_{0.54}Th_{0.46})O_2$ in air. The heating laser power was kept at 45 W in between the high-power pulses. The inset shows the solidification of the first heating/cooling cycle in more detail. The average solidification temperature of $(Pu_{0.54}Th_{0.46})O_2$ at 3208 K (calculated with a constant $\varepsilon = 0.846$) is suggested by the horizontal line, as well as the solidification temperature of the first cycle in the inset at 3220 K.

Figure 2 and table 1 summarise the solidification points observed with the different $(Pu,Th)O_2$ compositions investigated in this work. Single measured NSE values are also shown in table 1, which confirm within the uncertainty the assumption of interpolated values for the emissivity. For the calculation of the true solidification temperature the interpolated values were chosen.

Within the experimental uncertainty the temperature remains the same for the solidification of several successive shots, which indicates that segregation effects during the experiments seem to have only a minor influence. Due to the restricted number of samples, the resulting uncertainty is higher for Th-rich compositions. A composition with 70 mol% $ThO_2$ with only one available sample was also studied, but the thermal analysis was not successful due to malfunctioning pyrometers.

Interestingly $(Pu,Th)O_2$ solid solutions shows a minimum in the melting/solidification transition around 5 mol% $ThO_2$ content, similar to the $(U,Th)O_2$ [4].

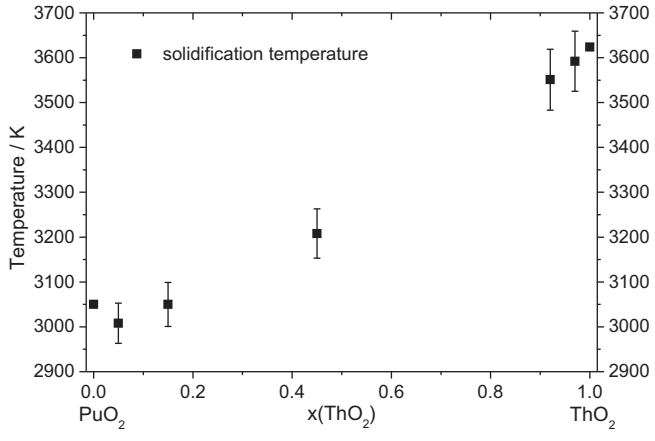


**FIGURE 2.** The average solidification temperatures determined at the thermal arrest for different mixed $(Pu,Th)O_2$. The uncertainties in temperature are determined in the thermal analysis.

### 3.2. Material characterisation

#### 3.2.1. Scanning electron microscopy

The laser irradiated sample surface was analysed with scanning electron microscopy at different magnifications. An example of such an analysis can be seen in figure 3. The re-solidified surface of a $(Pu_{0.85}Th_{0.15})O_2$ sample is shown. Cracks usually form during final cooling to room temperature. In back-scattered electrons (BSE) analysis only homogeneous material distribution on the surfaces is found. Energy-dispersive X-ray (EDX) analysis has relatively large uncertainties (±10% in absolute composition) considering the not-polished surfaces investigated here, and showed no changes in composition along the surface between re-solidified and not melted material.

#### 3.2.2. Raman spectroscopy

Raman measurements were conducted on the surface of the sample from the centre to the outside section, on re-solidified,

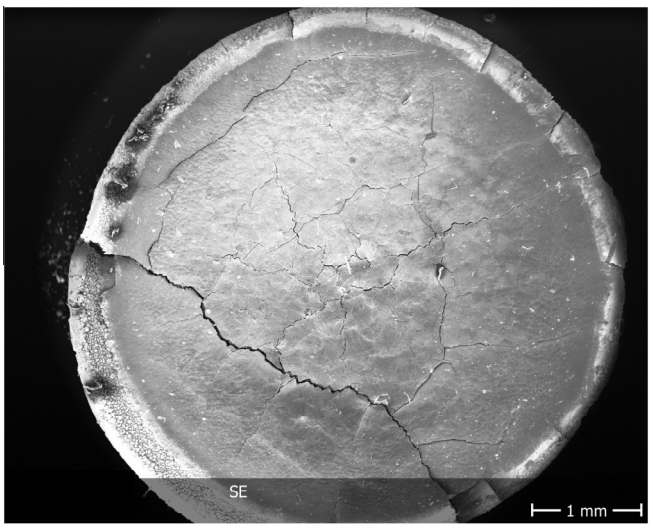


**FIGURE 3.** A secondary electron image of a $(Pu_{0.85}Th_{0.15})O_2$ sample after several heating/cooling cycles.

not melted, and fresh (not laser heated) material. The emission volume of the EDX is deeper than the expected penetration depth of the laser beam used in Raman spectroscopy as estimated with the Lamber–Beer law [4], so that possible surface effects are revealed better with the latter method.

The fluorite-like structures studied here (fcc, $Fm\bar{3}m$) have only one (triply degenerate) Raman active vibration ($T_{2g}$), which is taken as a reference peak for our investigation. In stoichiometric $PuO_2$ the peak is found at 478 $cm^{-1}$ and in thoria at 465 $cm^{-1}$ relative to the excitation wavelength [20]. The spectra of mixed, not melted $(Pu,Th)O_2$ show additional peaks as seen in figure 4. Spectra of $(Pu_{0.08}Th_{0.92})O_2$ of acceptable quality could not be obtained and were therefore not used in this comparison. In re-solidified material the peaks remained at the same position, as shown for the 46 mol% $ThO_2$ in figure 4.

The spectra in figure 4 are divided in three parts. Part I from (200 to 700) $cm^{-1}$, part II from about 2000–2200 $cm^{-1}$, part III from about (2500 to 2700) $cm^{-1}$. In part I the characteristic features for the investigated compounds are located which will be discussed here. One can identify a peak at approx. 260 $cm^{-1}$, which can be allocated to the LO mode, a weak mode at 335 $cm^{-1}$, and the $T_{2g}$ peak between (465 and 478) $cm^{-1}$, depending on the composition. The position of the latter is shown in more detail in figure 5.

This is followed by modes at about 535 $cm^{-1}$ (characteristic for hypostoichiometry [21]), around 575 $cm^{-1}$ (TO mode) and at about 630 $cm^{-1}$. The last was attributed in the case of uranium oxides to a $U_4O_9$ phase [21]. Part II and III show peaks which were also observed by Sarsfield *et al.* for pure $PuO_2$ [22]. Both peaks ("II" and "III") change position and become weaker with increasing $ThO_2$ content. Interestingly, the ratio between these and $T_{2g}$ is nearly constant as seen in table 2.

Especially interesting is the $T_{2g}$ peak position (figure 5), which is characteristic for each composition. Figure 5 presents the peak position for all compositions in dependence of the $ThO_2$ content from several measurements on the surfaces with different laser wavelength. Measurements taken on different spots were averaged since no differences were seen radially on the surface or from different samples with the same composition. The shift in position seems to depend linearly on the $ThO_2$ content of the samples. Since measurements with $(Pu_{0.08}Th_{0.92})O_2$ were not clearly interpretable, these results should be only considered with caution. A difference between the melted and not melted material could not be found, which suggests no change of composition during melting and re-solidification on the surface.

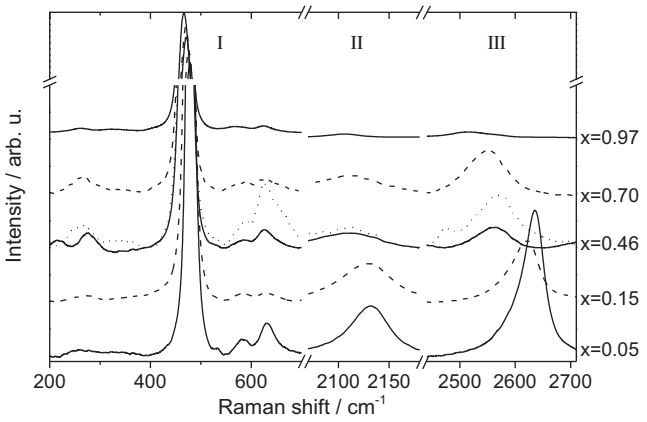


**FIGURE 4.** Single Raman spectra measured with 514 nm excitation wavelength on not melted material of different $(Pu_{1-x}Th_x)O_2$ compositions. The spectra are normalised to the $T_{2g}$ peak intensity and shown at 3 different wavenumber ranges. At $x(ThO_2) = 0.46$ the dotted line represents a re-solidified surface measurement.

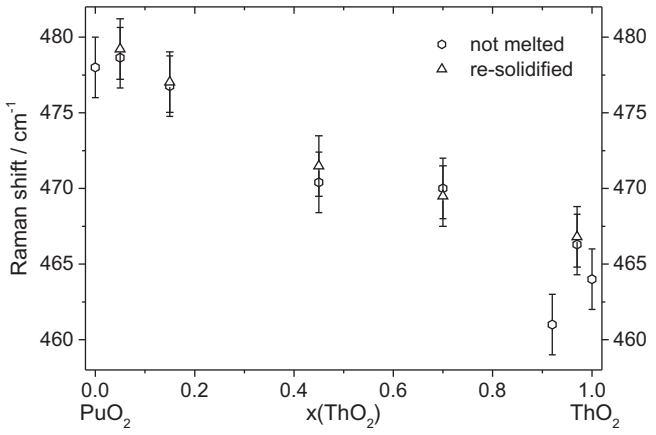


**FIGURE 5.** Raman $T_{2g}$ averaged peak positions (±2 $cm^{-1}$) in not melted (polygon) and re-solidified (triangle) $(Pu,Th)O_2$.

**TABLE 2**
The evolution of the Raman $T_{2g}$[a] and other peak positions with $ThO_2$ content in not melted $(Pu,Th)O_2$ measured at pressure $p = 0.1$ MPa.[a]

| Composition | Raman shift/$cm^{-1}$ | | | Raman shift ratios | |
|---|---|---|---|---|---|
| | $T_{2g}$ | "II" | "III" | "II"/$T_{2g}$ | "III"/$T_{2g}$ |
| $PuO_2$ | 478 | 2125 | 2629 | 4.45 | 5.50 |
| $(Pu_{0.95}Th_{0.05})O_2$ | 478.9 | 2130 | 2631 | 4.45 | 5.49 |
| $(Pu_{0.85}Th_{0.15})O_2$ | 476.9 | 2130 | 2620 | 4.47 | 5.49 |
| $(Pu_{0.54}Th_{0.46})O_2$ | 471.1 | 2112 | 2598 | 4.48 | 5.51 |
| $(Pu_{0.30}Th_{0.70})O_2$ | 469.7 | 2109 | 2547 | 4.49 | 5.42 |
| $(Pu_{0.08}Th_{0.92})O_2$ | 461 | | 2496 | | 5.41 |
| $(Pu_{0.03}Th_{0.97})O_2$ | 466.5 | 2104 | 2517 | 4.51 | 5.40 |
| $ThO_2$ | 464 | | | | |

[a] Standard uncertainties $u$ are $u(p) = 0.005$ MPa and $u(Raman\ shift) = 2$ $cm^{-1}$.

### 3.2.3. Powder X-ray diffraction

In addition bulk analyses was performed with XRD analysis to show influences on a larger scale. Figure 6 and table 3 show the lattice parameter obtained by Rietveld refinement of the diffraction pattern of the samples previously analysed by microscopy technique and Raman spectroscopy.

$PuO_2$ and $ThO_2$ are expected to form a solid solution and to follow Vegard's law. Not melted material in this work shows a positive deviation in nearly all compositions (see figure 6), but still

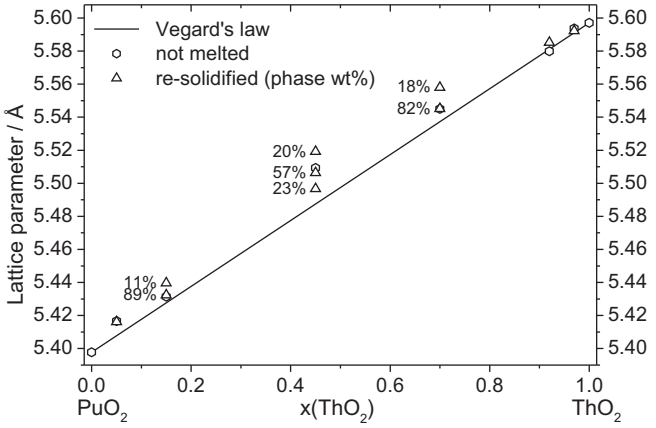


**FIGURE 6.** Lattice parameters for investigated $(Pu,Th)O_2$ compositions (±0.002 AA). Vegard's law is indicated by the straight line between the end-members. Re-solidified (triangles) and not melted material (polygon) are shown for measured samples. For cases with more than 1 phase, the numbers give the relative amount of each phase in weight percentage.

**TABLE 3**
Lattice parameters[a] of different (Pu,Th)$O_2$ compositions of not melted (and not-heated) and re-solidified material measured at pressure $p$ = 0.1 MPa.[a]

| Composition | Lattice parameter/Å | | | |
|---|---|---|---|---|
| | Not melted | Re-solidified | | |
| | | Main | 2nd | 3rd |
| $PuO_2$ | 5.3978 | | | |
| $(Pu_{0.95}Th_{0.05})O_2$ | 5.4167 | 5.4161 | 5.4165 | |
| $(Pu_{0.85}Th_{0.15})O_2$ | 5.4314 | 5.4324 | 5.4397 | |
| $(Pu_{0.54}Th_{0.46})O_2$ | 5.5093 | 5.5064 | 5.5192 | 5.4967 |
| $(Pu_{0.30}Th_{0.70})O_2$ | 5.5451 | 5.5452 | 5.5582 | |
| $(Pu_{0.08}Th_{0.92})O_2$ | 5.5799 | 5.5852 | | |
| $(Pu_{0.03}Th_{0.97})O_2$ | 5.5937 | 5.5922 | | |
| $ThO_2$ | 5.5971 | | | |

[a] Standard uncertainties $u$ are $u(p)$ = 0.005 MPa and $u$(*lattice parameter*) = 0.002 Å.

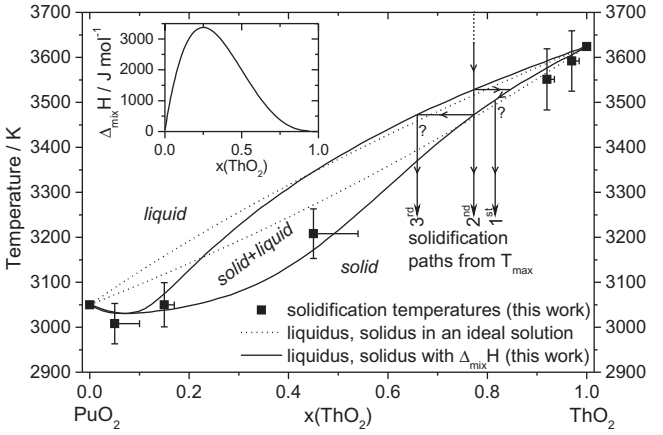


**FIGURE 7.** High temperature phase diagram of the pseudo-binary ($PuO_2$ + $ThO_2$) system. Composition uncertainties are deduced from and XRD measurements. Results of this work are shown together with the ideal solution binary solidus and liquidus (dotted lines). The solid solidus and liquidus lines take into account deviations from the ideal solution behaviour. They have been calculated by considering a mixing enthalpy in the solid solution, whose values reported in the inset have been optimised in order to best fit the current experimental data with a polynomial formalism as shown in equation (1). Possible segregation to 3 phases is shown by theoretical solidification paths from high temperature.

follows the trend of Vegard's law. Such deviation is also visible in other work with mixed actinide dioxides presenting the lattice parameter. In the work of Hubert *et al.* [23] the lattice parameter deviates up to 0.015 Å from Vegard's law for (Pu,Th)$O_2$, which is about the same deviation found in this work.

For the sample containing 46 mol% $ThO_2$, a phase separation into three fcc phases is observable after melting, but the most abundant phase remains similar to the fresh material. The re-solidified material in other intermediate compositions shows a also phase separation, but only into two phases. The most abundant phase still remains for all compositions similar to the fresh and not melted material.

## 4. Discussion

The accuracy with which a phase diagram is experimentally determined depends on two main issues: the accuracy in the measurement of temperature and the accuracy in the characterisation of the sample composition at the exact moment when the phase transitions occur. In the following section, first the impact of the melting experiments and the material analysis is discussed. Afterwards the phase diagram of (Pu,Th)$O_2$ is critically revisited.

### 4.1. Melting temperature results

Only one assessment of the ($PuO_2$ + $ThO_2$) phase diagram as a pseudo-binary system exists so far [6]. With newer data for $PuO_2$, this assessment was updated. The results in the present study for intermediate compositions are in reasonable agreement with former work on the pure end members [18,17].

Considering results from Phase-Field simulation of such laser heating experiments [4,3,19], the temperature at the thermal arrest or peak (see figure 1) was determined to be the point when the surface has completely resolidified. Therefore it is reasonable to equalise the solidification temperature of this work with a solidus.

The melting temperatures of the $ThO_2$-rich compositions follow closely the solidus calculated with an ideal solution assumption (see figure 7). Also in the earlier assessment [6] this trend was visible. But only compositions with a $ThO_2$ content up to 70 mol% were investigated before.

The $PuO_2$-rich compositions show a deviation from the ideal binary solution with the minimum around a 5 mol% $ThO_2$ content, as it was already reported for other mixed actinide oxides [3,4]. Due to its comparatively high oxygen potential among the actinide oxides, plutonium dioxide may be more easily reduced, and therefore an assumption of a stoichiometric pseudo-binary section may not be fully suitable in this region. The material analysis has not shown any deviation which could account completely for this behaviour. The Raman surface analysis has shown possible lattice defects, maybe resulting from a small hypostoichiometry of the sample. But the material analysis was conducted at room temperature after the experiments. Changes in the material which are found later in the analysis are probably quenched from high temperature. In-situ effects at high temperature, such as possible reversible or temporarily oxygen losses, cannot be seen by any material analysis.

Moreover, one observes segregation effects by the XRD analysis, which probably took place at high temperature, and were partially quenched to room temperature. The phase analysis showed up to three distinct phases, which should have hence a distinct measurable phase transition temperature, if they crystallise from the liquid on the surface. In the thermograms these effects are not observable as different solidification arrest or clear inflections. The proportion of new appearing phases is small and therefore the latent heat released by this new phase will be also small. The reflected light signal technique only showed one phase change during cooling. As well, the location of this segregation cannot be determined exactly in the molten pool or later in the re-solidified material. At the surface, where the temperature is measured, the material analysis by Raman spectroscopy has not shown signs of segregation, so that also the uncertainties in composition for the phase transition are taken from the uncertainties from the XRD analysis for the most abundant phase at each composition in re-solidified material.

### 4.2. Material characterisation

#### 4.2.1. Microscopy

Within the uncertainty of the EDX and BSE analyses, no differences in composition of not melted and re-solidified material or a phase separation was found on any sample at different magnifications. Any segregation effects as seen by the XRD results seem to not occur close to the surface. However, with this analysis method small differences are difficult to determine and might not be detected.

#### 4.2.2. Raman spectroscopy

An analysis of the composition can be done with the Raman $T_{2g}$ vibration, whose shift is proportional to the $ThO_2$ content (figure

5). For mixed crystals, it has been estimated already with the random-element-isodisplacement model (REI) [24], that the optic mode frequency varies continuously and approximately linearly with concentration from the frequency characteristic of one end member to that of the other end member in a one-mode behaviour. Re-solidified and not melted material showed in all samples and compositions nearly no difference for the $T_{2g}$ position. Thus, no segregation effects can be deduced from this analysis on the surface of the samples.

The Raman spectra show further modes (figure 4). The LO (at 260 $cm^{-1}$) and TO (575 $cm^{-1}$) modes are normally only visible by IR spectroscopy and become Raman active only if the lattice is disordered. These observed peaks therefore indicate defects in the lattice, which can be linked to energetically favourable oxygen Frenkel defects or oxygen losses, possibly quenched to room temperature. Also the peaks at 535 and 630 $cm^{-1}$ can be related to a disorder in the lattice, while a formation of $M_4O_9$ with these compounds, as in uranium compounds [21], seems unlikely. The origin of the band around 335 $cm^{-1}$ remains unclear.

The modes at higher energy (around 2100 and 2600 $cm^{-1}$) seem to be related to the composition and obviously to $PuO_2$. Sarsfield *et al.* [22] extensively discussed the origin of these peaks, ruling out interactions with the surrounding atmosphere and material, and suggesting an electronic origin with energies of about (262 and 324) meV respectively. The nearly constant ratio observed at different compositions between the $T_{2g}$ and the higher energy peaks (see table 2) tempt one to see a relationship between these modes. If these peaks were a combination of $T_{2g}$ with another transition or vibration, these should be visible in the measured spectra. But no other modes were found in the spectra which had the required wavenumbers. Hence, no combinations can be so far clearly attributed to the high energy peaks in these spectra, and the origin(s) of these signals remain unclear.

*4.2.3. Powder X-ray diffraction*

The powder X-ray diffraction analysis was used to determine lattice constants of different samples. Deviations from Vegard's law in the lattice parameters could have several reasons: (i) composition shifts, (ii) defects, or (iii) stoichiometry changes. It is not possible to distinguish them only with the lattice parameter data, so that the influences have to be discussed separately but all may be present together as presented for (iv) the phase separation found in this work. In general, the re-solidified material could also be contaminated with not-melted material, which might also result in multiple phases due to a difficult separation during the preparation for the powder X-ray diffraction analysis.

(i) A deviation of the lattice parameter in not heated or not melted samples could be caused by inaccuracy in composition during the sample preparation, as seen in other work with $(Pu,Th)O_2$ [23]. The deviation of the most abundant phase after melting is assumed as a worst-case uncertainty source for the solidification temperature in figure 2, resulting in error bars towards the $ThO_2$ side of the phase diagram.

(ii) Defect formation due to age would increase the lattice parameter [22]. Additionally, more defects due to other origin than a self-irradiation may be introduced at higher temperature and quenched to room temperature. Small deviations from Vegard's law could be related to this issue.

(iii) A change in stoichiometry inducing a lattice expansion is difficult to quantify. Different studies on hypostoichiometric actinide dioxides suggest a lattice swelling [1,25], but there is no data so far for mixed $(Pu,Th)O_2$. The expansion rate of the lattice of $(Pu,Th)O_{2-y}$ can be approximated from literature data of other dioxides [1,4] to 0.04 Å per $y = 0.1$, leading to only limited hypostoichiometry for all compositions (maximum at the 2nd phase of $(Pu_{0.54}Th_{0.46})O_{1.93}$ compared to fresh material $(Pu_{0.54}Th_{0.46})O_{1.96}$). Melting of the material seems not to have an strong influence on stoichiometry, since all re-solidified samples have a very similar lattice parameter compared to not melted material. Nevertheless, a slight hypostoichiometry of the samples cannot be excluded, especially since the rather complicated Raman spectra of these compositions also show signs of a disturbed lattice, which can be linked to oxygen losses.

(iv) Considering only stoichiometric changes and disregarding changes in composition, the phase separation seen in intermediate compositions, could be interpreted as a phase close to stoichiometry and two phases more reduced. This would also imply that the initial, fresh material is either not stoichiometric and/or has a different composition. A change to a hyperstoichiometric phase in $PuO_2$-rich compositions, as one might expect from the higher oxygen potential of $PuO_2$ compared to $ThO_2$, was not found. A reduction as seen by Truphmus *et al.* [26] to three distinct phases for non-stoichiometric $(U,Pu)O_2$ could not be seen in that extent for $(Pu,Th)O_2$. To explain the effects seen in this study only with oxygen related phenomena, one has to assume a slightly non stoichiometric section in the (Pu + Th + O) phase diagram as already suggested for mixed $(U,Pu)O_2$ [27,1], with a miscibility gap for non-stoichiometric material only for intermediate compositions. Therefore only oxygen defects, quenched from high temperature to room temperature, could be partly accountable for the lattice parameter changes whereas these are unlikely to cause a phase separation.

But the appearance of more phases can be also linked to a segregation upon melting or freezing process. Phases, enriched and reduced with material with the higher melting point, can be explained in terms of segregation effects during cooling and solidification of the material with the help of the binary phase diagram (figure 7)). If the cooling process is fast enough compared to the diffusion processes, quenching of the high temperature phases is possible. When material solidifies with an enriched composition (1st solidified phase), the remaining melt is equally depleted in composition. If there is not enough time to regain the initial composition by diffusion, a new phase would appear with a depleted composition. But if the solidification happens quickly enough, there is even not enough time to reach a homogeneous melt depleted in composition compared to the initial material and three phases might form, with a phase equal to the initial material (2nd solidified phase) and depleted in composition (3rd solidified phase). The phase separation happens presumably only at the solidification front, which are supposedly located at the edges of the molten pool [3]. Because it was not possible to select the samples for the XRD material analysis by these criteria, the amount of phases and weight of the enriched and reduced phases is not always found to be the same.

Other investigated mixed actinide dioxides showed no segregation ($(U,Pu)O_2$ [3]) or in much less extent ($(U,Th)O_2$ [4]). This can be explained with the binary phase diagrams. Since the melting temperatures of the end members are closer to each other in the latter cases, segregation is less probable, because the liquidus and solidus points are also closer together. The composition which solidifies the first is nearby the initial composition and may be not seen in any material analysis method.

Segregation to different phases was not seen by a shift of the $T_{2g}$ position in the Raman analysis nor in the microstructure analysis. All observed phases have a fcc structure, which makes it more difficult to see small deviations introduced by a small composition change. In the case of $(U,Th)O_2$,

segregation effects were also seen in the Raman analysis [4]. If these changes only affect the material close to the surface, they are very likely to be overseen or averaged out with powder diffraction analysis method and are very difficult to locate.

### 4.3. Phase diagram considerations

In the hypothetical case of no interaction between the solution end-members, assuming that the heat capacity is approximately the same for solid and liquid phases in the vicinity of melting, and taking into account that the only entropy contributions to Gibbs free energy are related to configurational terms, the ideal-solution solidus and liquidus lines of the binary phase diagram are solely defined by the melting temperatures and the enthalpies of fusion of the two end members [28] as shown by the dotted lines in figure 7. Actinide dioxide melting enthalpy values assessed by Konings *et al.* [29] are used to calculate the optimised solidus and liquidus plotted in figure 7 together with the current experimental data. It is evident that the current experimental data relative to plutonia-rich compositions deviate from such phase diagram. Therefore, the system cannot be represented by considering only an ideal behaviour of both solid and liquid solutions.

Deviations from ideality, can be related to various factors, as for example lattice strain caused by a difference in the ionic radii of $Pu^{4+}$ and $Th^{4+}$, or a different oxygen potential of the pure end members [3]. Recent research [3,1] has shown that the latter point plays an important role in the very high temperature behaviour of these oxides, especially around the melting transition. It has been reported [30], that pure plutonium dioxide melts congruently at a slightly hypostoichiometric composition ($PuO_{1.98\pm0.02}$). Therefore, mixed oxides including plutonium dioxide cannot be rigorously treated as purely pseudo-binary ($(M_1^{4+}, M_2^{4+})O_2$), but are thermodynamically more accurately described as ternary systems ($(M_1^{4+}, M_2^{4+}, M_2^{3+})O_2$). This behaviour, thoroughly assessed for the system (U + Pu + O) [30], should certainly apply also to the current system (Pu + Th + O). However, a full thermodynamic assessment of the ternary (Pu + Th + O) system goes beyond the scopes of the present work, and will be left for further investigation. Therefore, as a first approximation, the solidus and liquidus lines are optimised here, according to the current experimental data, in the pseudo-binary ($PuO_2 + ThO_2$) plane in the rough assumption that $PuO_2$ does melt congruently. By considering excess Gibbs free energy terms instead of an ideal solution, one can find the best data fit in a pseudo-binary plane, including the minimum melting point around $x(ThO_2) = 0.05$, following an approach similar to that proposed by Pelton and Thompson [31]. The following expression has thus been used for the excess Gibbs free energy of the solid phase:

$$\Delta G^{exc}(x(ThO_2)) = x(PuO_2)^3 \cdot x(ThO_2) \cdot \Omega. \quad (1)$$

$x(ThO_2)$ and $x(PuO_2)$ are the mole fractions of $ThO_2$ and $PuO_2$, respectively. $\Omega$ is the non-ideal interaction energy term between $PuO_2$ and $ThO_2$, assumed to be a temperature-independent parameter. In equation (1), $\Delta G^{exc}$ coincides with the excess enthalpy in the non-ideal solution model, as excess entropic contributions have been neglected. $x(PuO_2)$ appears at the third power to account for asymmetry of the model, according to the fact that deviations from the ideal solution behaviour, and in particular a minimum melting point, have been mostly observed in $PuO_2$-rich compositions. In the current model, the interaction parameter $\Omega$ is considered to be zero in the liquid phase (non-ideality is neglected in the liquid).

The resulting optimised solidus and liquidus lines are plotted in figure 7 together with the current experimental data points. The corresponding best value for the interaction parameter is $\Omega = 36\ kJ \cdot mol^{-1}$, yielding the excess mixing enthalpy, $\Delta_{mix}H$, plotted in the inset of figure 7. The minimum melting point can be reasonably fitted with the current approach, as well as the other experimental data points, within the reported uncertainty bars. The approximations adopted in the current phase boundary optimisation are somewhat coarse, because they imply that plutonium dioxide melts congruently and, moreover, neglect non-ideality parameters in the liquid phase. Nonetheless, the fair quality of the present data fit permits to quantify, roughly, the non-ideality of the alleged pseudo-binary system, whereby even changes in oxygen stoichiometry (outside the ($PuO_2 + ThO_2$) pseudo-binary plane) can be accounted for as deviations from ideality. Thus, the modest values of the current excess solution enthalpy show that the minimum melting point observed for just a few mol% of $ThO_2$ dissolved in $PuO_2$ can be justified even with small deviations from an ideal behaviour of the pseudo-binary system. Such deviations can be most probably related, in a more detailed approach, to the formation of oxygen defects, and in particular oxygen losses, due to the high oxygen potential of plutonium dioxide and $PuO_2$-rich compositions at temperatures close to melting. This is in line with the material characterisation in this work which shows signs of hypostoichiometry in the samples. As mentioned above, a non-stoichiometric phase diagram as already suggested for $(U,Pu)O_{2\pm y}$ by a full CALPHAD optimisation [30], seems a reasonable assumption for the description of melting in the $(Pu,Th)O_2$ system, too. In addition, a similar melting behaviour has recently been assessed also for the $(U,Th)O_2$ system [4]. There, however, uranium has a more complex chemistry than plutonium, permitting the accommodation of both oxygen vacancies (valence state $U^{3+}$) and interstitials ($U^{5+}$, $U^{6+}$). This makes the high temperature behaviour more difficult to estimate in (uranium + thorium) mixed dioxides [4]. Finally, in the light of these observations, it is suggested that also the (plutonium dioxide + thorium dioxide) system can only be fully understood with an assessment of the ternary (Pu + Th + O) system rather than a simplified pseudo-binary section.

## 5. Conclusions

With new laser-heating results on the melting transition, the high temperature phase diagram of mixed (plutonium + thorium) dioxides has been assessed in the present work. Large deviations from the few earlier results are reported. With the material characterisation performed before and after melting by SEM, Raman spectroscopy and XRD, phase separation processes in relation with the phase diagram were identified and explained. Additionally, new observations of high energy Raman modes are presented and related to $PuO_2$.

As with other mixed actinides dioxides, mixed plutonium-thorium dioxides show a minimum melting point. Such a minimum occurs in plutonium dioxide-rich compositions (around 95 mol%) at a temperature close to 3000 K. Moreover, the current observations lead to the conclusion that such effects can only be fully understood within a comprehensive study of the ternary (Pu + Th + O) system. The material analyses performed here support this interpretation by yielding signs of oxygen losses for several compositions. These results emphasise that knowledge and control of the oxygen potential in the investigation of the actinide dioxides is crucial, especially at high temperatures.

## Acknowledgements

The Authors are indebted to the JRC – ITU members G. Pagliosa, D. Bouexire, B. Cremer, A. Janssen and O.S. Valu for their precious help in the sample characterisation and P. Raison and A.L. Smith for the helpful discussions and valuable suggestions. This work is

funded by the European Commission and partly supported by E.ON Kernkraft GmbH via contract No. 32920.

## References

[1] C. Guéneau, A. Chartier, L.V. Brutzel, 2.02 – Thermodynamic and thermophysical properties of the actinide oxides, in: R.J. Konings (Ed.), Comprehensive Nuclear Materials, Elsevier, Oxford, 2012, pp. 21–59, http://dx.doi.org/10.1016/B978-0-08-056033-5.00009-4.
[2] O. Vălu, O. Beneš, R. Konings, H. Hein, J. Chem. Thermodyn. 68 (2014) 122–127, http://dx.doi.org/10.1016/j.jct.2013.08.017.
[3] R. Böhler, M. Welland, D. Prieur, P. Çakır, T. Vitova, T. Pruessmann, I. Pidchenko, C. Hennig, C. Guéneau, R. , D. Manara, J. Nucl. Mater. 448 (1–3) (2014) 330–339, http://dx.doi.org/10.1016/j.jnucmat.2014.02.029.
[4] R. Böhler, A. Quaini, L. Capriotti, P. Çakır, O. Beneš, K. Boboridis, A. Guiot, L. Luzzi, R. Konings, D. Manara, J. Alloys Compd. 616 (2014) 5–13, http://dx.doi.org/10.1016/j.jallcom.2014.07.055.
[5] H. Kinoshita, D. Setoyama, Y. Saito, M. Hirota, K. Kurosaki, M. Uno, S. Yamanaka, J. Chem. Thermodyn. 35 (5) (2003) 719–731, http://dx.doi.org/10.1016/S0021-9614(03)00002-8.
[6] K. Bakker, E. Cordfunke, R. Konings, R. Schram, J. Nucl. Mater. 250 (1) (1997) 1–12, http://dx.doi.org/10.1016/S0022-3115(97)00241-9.
[7] R. Agarwal, S.C. Parida, Phase diagrams and thermodynamic properties of thoria, thoria–urania, and thoria–plutonia, in: D. Das, S.R. Bharadwaj (Eds.), Thoria-based Nucl. Fuels, Green Energy and Technology, Springer, London, 2013, pp. 71–105, http://dx.doi.org/10.1007/978-1-4471-5589-8.
[8] F. De Bruycker, K. Boboridis, D. Manara, P. Pöml, M. Rini, R.J. Konings, Mater. Today 13 (11) (2010) 52–55, http://dx.doi.org/10.1016/S1369-7021(10)70204-2.
[9] C. Lombardi, L. Luzzi, E. Padovani, F. Vettraino, Prog. Nucl. Energy 38 (3–4) (2001) 395–398, http://dx.doi.org/10.1016/S0149-1970(00)00143-8.
[10] J. Somers, D. Papaioannou, J. McGinley, D. Sommer, J. Nucl. Mater. 437 (1–3) (2013) 303–309, http://dx.doi.org/10.1016/j.jnucmat.2013.02.046.
[11] P.R. Hania, F.C. Klaassen, 3.04 – Thorium oxide fuel, in: R.J.M. Konings (Ed.), Comprehensive Nuclear Materials, Elsevier, Oxford, 2012, pp. 87–108, http://dx.doi.org/10.1016/B978-0-08-056033-5.00052-5.
[12] C. Cozzo, D. Staicu, J. Somers, A. Fernandez, R. Konings, J. Nucl. Mater. 416 (1–2) (2011) 135–141, http://dx.doi.org/10.1016/j.jnucmat.2011.01.109.
[13] Thematic network on advanced options for partitioning and transmutation (ADOPT), Tech. rep., European Commission, 2005.
[14] Oxide fuels: microstructure and composition variations (OMICO), Tech. rep., European Commission, 2007.
[15] D. Manara, C. Ronchi, M. Sheindlin, M. Lewis, M. Brykin, J. Nucl. Mater. 342 (1–3) (2005) 148–163, http://dx.doi.org/10.1016/j.jnucmat.2005.04.002.
[16] D. Manara, M. Sheindlin, W. Heinz, C. Ronchi, Rev. Sci. Instrum. 79 (11) (2008) 113901, http://dx.doi.org/10.1063/1.3005994.
[17] C. Ronchi, J.-P. Hiernaut, J. Alloys Compd. 240 (1–2) (1996) 179–185, http://dx.doi.org/10.1016/0925-8388(96)02329-8.
[18] F. De Bruycker, K. Boboridis, P. Pöml, R. Eloirdi, R. Konings, D. Manara, J. Nucl. Mater. 416 (1–2) (2011) 166–172, http://dx.doi.org/10.1016/j.jnucmat.2010.11.030.
[19] R. Böhler, M.J. Welland, F.D. Bruycker, K. Boboridis, A. Janssen, R. Eloirdi, R.J.M. Konings, D. Manara, J. Appl. Phys. 111 (11) (2012) 113501, http://dx.doi.org/10.1063/1.4721655.
[20] G. Begun, R. Haire, W. Wilmarth, J. Peterson, J. Less Common Met. 162 (1) (1990) 129–133, http://dx.doi.org/10.1016/0022-5088(90)90465-V.
[21] L. Desgranges, G. Baldinozzi, P. Simon, G. Guimbretière, A. Canizares, J. Raman Spectrosc. 43 (3) (2012) 455–458, http://dx.doi.org/10.1002/jrs.3054.
[22] M.J. Sarsfield, R.J. Taylor, C. Puxley, H.M. Steele, J. Nucl. Mater. 427 (1–3) (2012) 333–342, http://dx.doi.org/10.1016/j.jnucmat.2012.04.034.
[23] S. Hubert, J. Purans, G. Heisbourg, P. Moisy, N. Dacheux, Inorg. Chem. 45 (10) (2006) 3887–3894, http://dx.doi.org/10.1021/ic050888y.
[24] I. Chang, S. Mitra, Phys. Rev. 172 (3) (1968) 924–933, http://dx.doi.org/10.1103/PhysRev. 172.924.
[25] J.M. Haschke, T.H. Allen, L.A. Morales, Science 287 (5451) (2000) 285–287, http://dx.doi.org/10.1126/science.287.5451.285.
[26] T. Truphémus, R.C. Belin, J.-C. Richaud, M. Reynaud, M.-A. Martinez, I. Félines, A. Arredondo, A. Miard, T. Dubois, F. Adenot, J. Rogez, J. Nucl. Mater. 432 (1–3) (2013) 378–387, http://dx.doi.org/10.1016/j.jnucmat.2012.07.034.
[27] C. Sari, U. Benedict, H. Blank, J. Nucl. Mater. 35 (3) (1970) 267–277, http://dx.doi.org/10.1016/0022-3115(70)90211-4.
[28] M. Kato, K. Morimoto, H. Sugata, K. Konashi, M. Kashimura, T. Abe, J. Nucl. Mater. 373 (1–3) (2008) 237–245, http://dx.doi.org/10.1016/j.jnucmat.2007.06.002.
[29] R.J.M. Konings, O. Beneš, A. Kovács, D. Manara, D. Sedmidubský, L. Gorokhov, V.S. Iorish, V. Yungman, E. Shenyavskaya, E. Osina, J. Phys. Chem. Ref. Data 43 (1) (2014) 013101, http://dx.doi.org/10.1063/1.4825256.
[30] C. Guéneau, N. Dupin, B. Sundman, C. Martial, J.-C. Dumas, S. Gossé, S. Chatain, F.D. Bruycker, D. Manara, R.J. Konings, J. Nucl. Mater. 419 (1–3) (2011) 145–167, http://dx.doi.org/10.1016/j.jnucmat.2011.07.033.
[31] A. Pelton, W. Thompson, Prog. Solid State Chem. 10 (1975) 119–155, http://dx.doi.org/10.1016/0079-6786(75)90004-7.

JCT 14-403